doi: 10.1038/nature06739

MOLECULAR IDENTIFICATION OF A NOVEL RETINAL CELL TYPE THAT RESPONDS TO UPWARD MOTION

In-Jung Kim, Yifeng Zhang, Masahito Yamagata, Markus Meister and Joshua R. Sanes
Department of Molecular and Cellular Biology and Center for Brain Science
Harvard University, Cambridge MA, 02138, USA

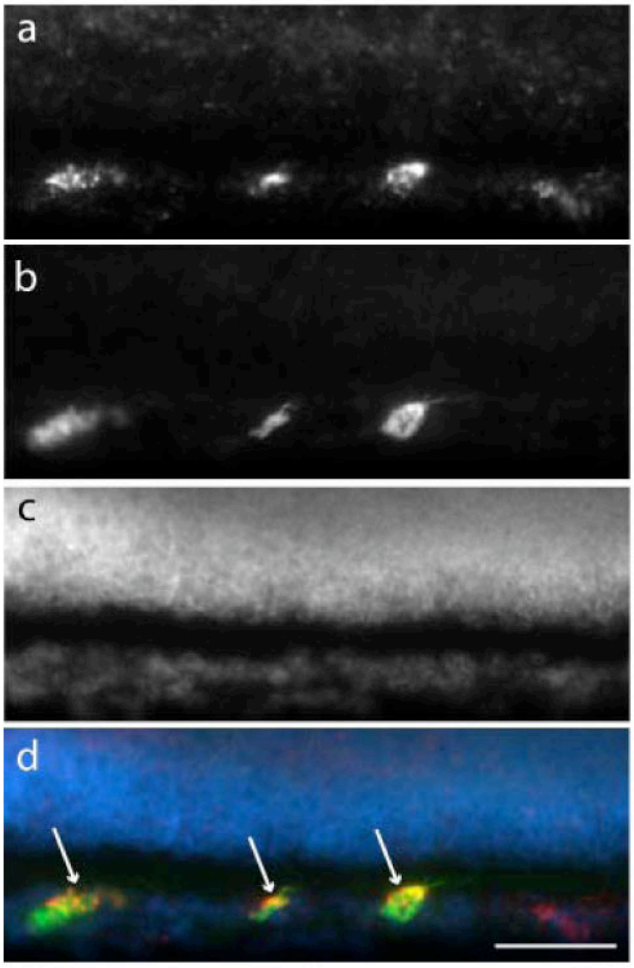

Supplementary Figure 1. Section of JAM-B-CreER;Thy1-STOP-YFP double transgenic retina probed by in situ hybridization for *JAM-B* (**a**) and by immunostaining for YFP (**b**). **c.** DAPI (nuclear) stain. **d.** Merge. Bar is 50 μm.

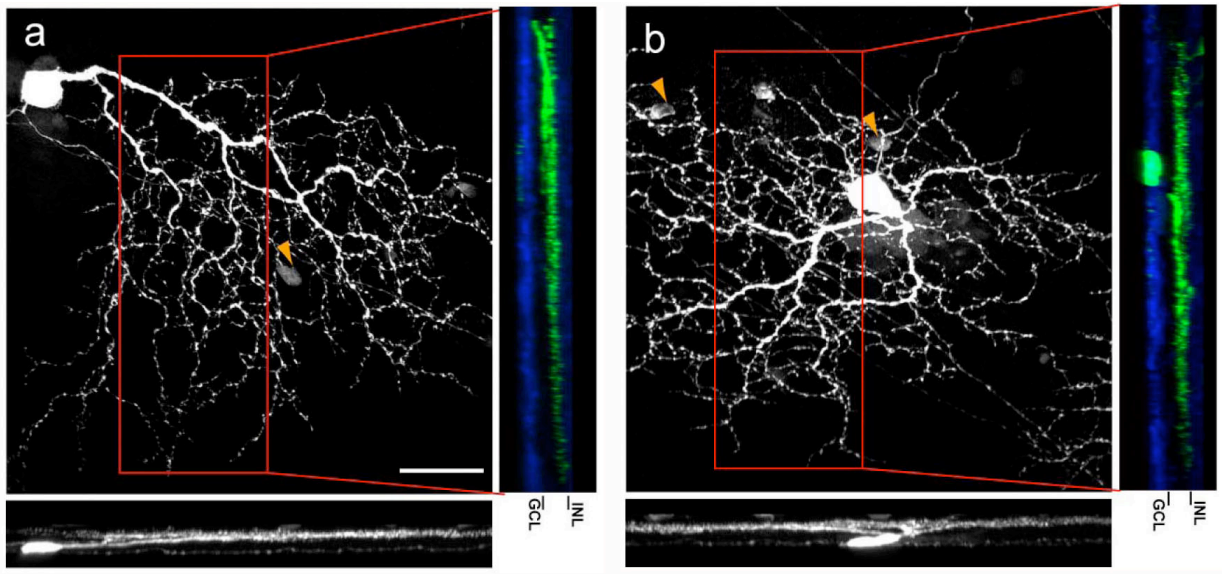

Supplementary Figure 2. Confocal reconstructions of an asymmetrical J-RGC near the center of a retina (**a**) and a symmetrical J-RGC near the ventral margin of the retina (**b**). Ninety degree rotations of the image stacks (boxed region at right and whole image at bottom) show that dendrites of both asymmetrical and symmetrical J-RGCs arborize in the outer portion of the IPL. Previously described ON- and ON-OFF direction-selective mouse ganglion cells[38,39] differ from those described here: their dendrites are less asymmetrical and arborize in different IPL sublaminae. Some amacrine cells also expressed YFP in JAM-B-CreER;Thy1-STOP-YFP double transgenic mice (arrowheads in **b**; see also show Figs. 1e and Supplementary Fig. 3e), but these cells expressed little if any endogenous *JAM-B*, as assessed by in situ hybridization. We suspect their labeling reflects ectopic expression of CreER from the transgene. Scale bar is 50 μm.

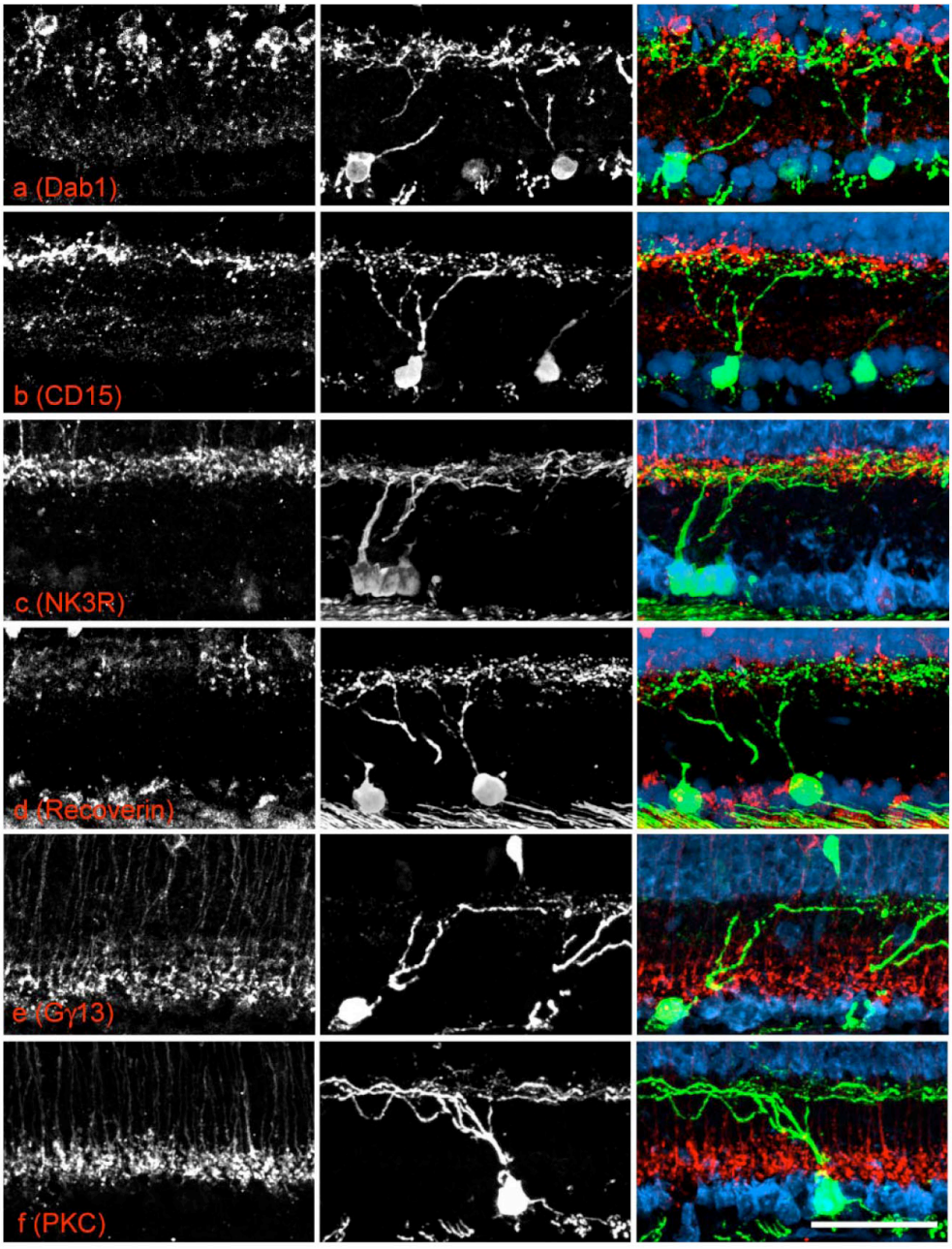

Supplementary Figure 3. Sections of retinae from JAM-B-CreER;Thy1-STOP-YFP mice were double labeled with antibodies to GFP (middle panels and green in right panels) and cell type-specific markers (left panels and red in right panels). **a.** Dab1 labels type IIA amacrines[35]. **b.** CD15 labels a subset of amacrines known to arborize near the inner nuclear layer[36]. **c.** Neurokinin-3 receptor marks OFF bipolar type 1 and 2 cells. **d.** Recoverin labels type 2 OFF bipolar cells. **e.** Gγ13 labels ON bipolar cells. **f.** PKC marks ON rod bipolar cells. Scale bar is 50 μm.

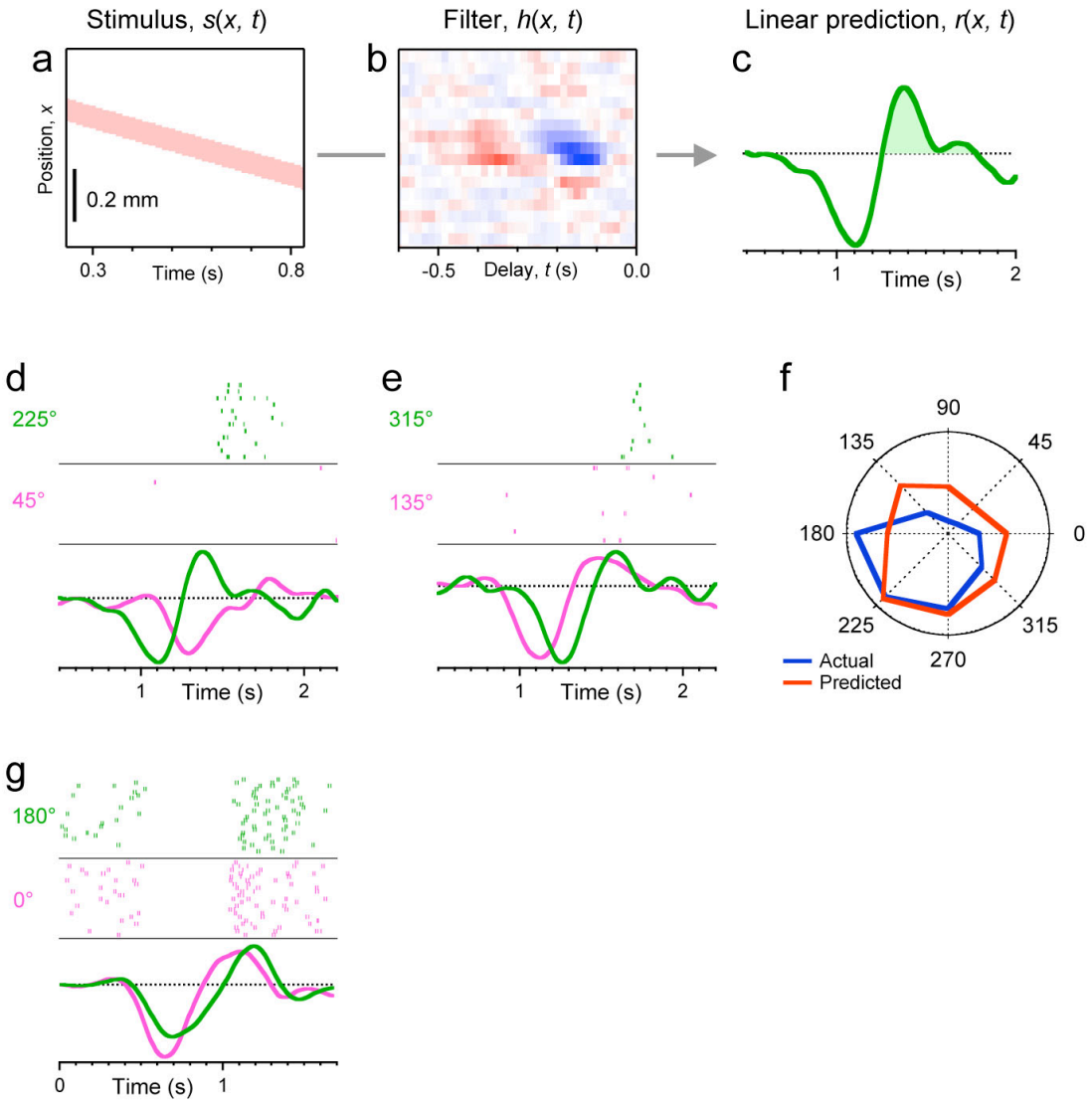

Supplementary Figure 4. Linear model of the ganglion cell response to moving spots. **a.** Space-time diagram $s(x,t)$ of a 115-μm wide bright spot moving in the x-direction at 575 μm/s. **b.** Spatio-temporal receptive field $h(x,t)$ of a J-RGC, computed from a strip of flickering bars along the same direction (see Fig 3a, b). **c.** In a linear approximation of the neuron's behavior[20], the time-reverse of the receptive field, $h(x,-t)$ can be interpreted as the impulse response of the cell's firing rate to a brief flash at position *x* and time *t*. Thus a linear prediction $r(x,t)$ of the

response to the moving spot is obtained by convolving $s(x,t)$ with $h(x,-t)$: $r(x,t) = \iint_{x\ t'} s(x,t') \cdot h(x,t'-t)\,dt'dx$. The initial negative overshoot occurs when the bright spot enters the cell's OFF receptive field center. The subsequent positive peak results when the spot leaves the OFF center and enters the ON surround. To predict the cell's firing rate, which is necessarily positive, this linear response must be rectified by some non-linear transform, such as the half-wave rectification illustrated by the shaded portion. **d.** Comparison of the measured spike trains obtained from two opposite directions of spot motion (raster graphs of multiple trials at top and middle) with the predicted responses $r(x,t)$ (bottom). For one direction (225°) the prediction makes a large positive excursion, and indeed the neuron fires many spikes; for the opposite direction (45°) the prediction barely crosses into positive values, and only few spikes are observed. **e.** As in panel d, for the orthogonal directions of motion. Here the predicted response is almost equally large for both directions, and indeed they produce similar spike numbers. Note $r(x,t)$ predicts that the response to 135° should begin earlier than to 315°, and indeed this occurs in the actual spike trains. **f.** Actual and predicted response of this J-RGC to the 8 directions. We performed this analysis on 6 J-RGCs for which all the required experiments could be performed. In each case we computed the preferred direction from the actual and the predicted responses, as described in Methods. The average discrepancy between the actual preferred direction and that predicted from a linear model was 47°. **g.** Comparison of measured spike trains and predicted responses to two opposite directions for a symmetric J-RGC. This neuron had a maintained firing rate at rest, which better illustrates the correspondence between actual and predicted responses. The initial negative transient in the prediction is matched by a sharp suppression of firing. The subsequent positive lobe of the prediction corresponds to a sharp increase in firing, which then declines back to the resting level. Note the predicted response peak for 0° occurs earlier than for 180°, and this is also observed in the actual response.

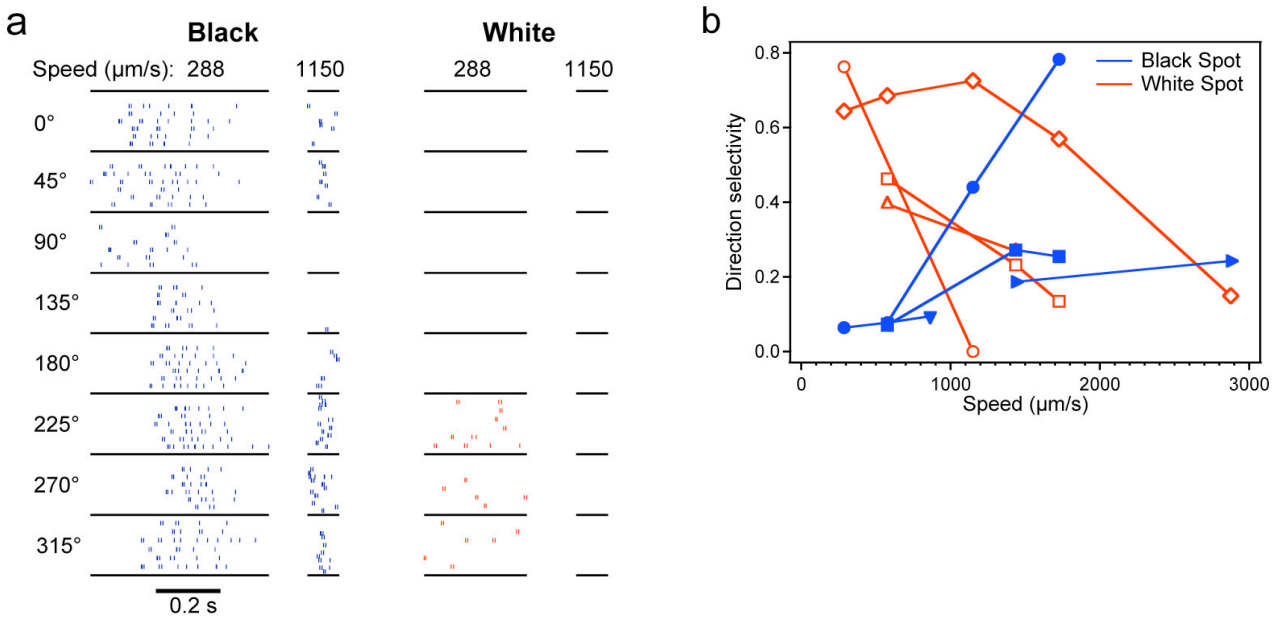

Supplementary Figure 5. Responses to black and white spots at different speeds. **a.** Sample responses from one J-RGC to spots moving in 8 different directions. The spot was either black (left) or white (right), and moved at low speed (288 μm/s) or high speed (1150 μm/s). For each condition, spike trains from several trials are shown in a raster plot. At low speed, the spot takes longer to traverse the receptive field, and thus the period of firing is longer as well. Note that the response to the black spot was more direction-selective at high speeds than at low speeds. By contrast, the response to the white spot was direction-selective at low speeds and failed entirely at high speeds. The preferred direction was almost identical under all conditions. **b.** Direction selectivity index (see Fig. 3h and Methods) obtained using white spots (open symbols) and black spots (closed symbols) at various speeds. Results from 6 J-RGCs denoted with different symbol shapes. Note that the response is more direction-selective at low speeds with white spots, but at high speeds with black spots. This accords with predictions derived from the spatio-temporal receptive field (Fig. 3b).

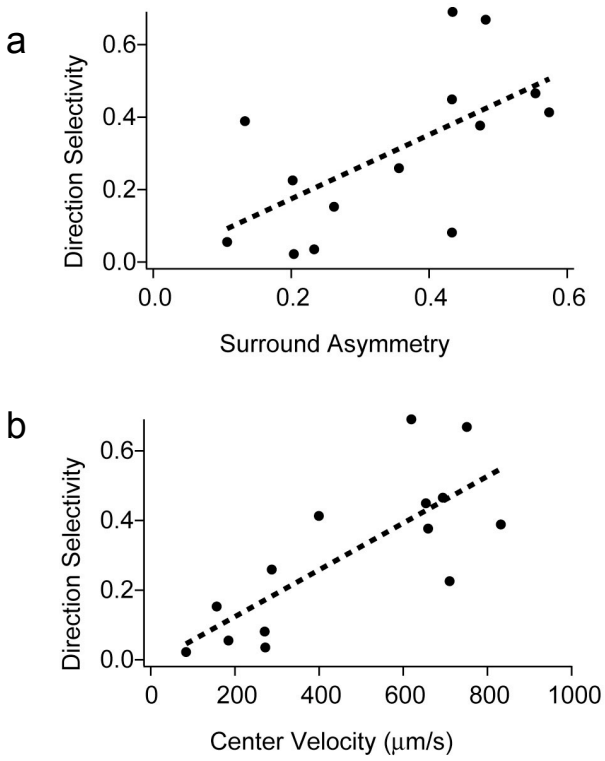

Supplementary Figure 6. Correlations between three measures of functional asymmetry in the population of J-RGCs. The strength of direction selectivity to moving spots (D , Eqn 2) is plotted against the degree of surround asymmetry (A , Eqn 8) in panel **a** and the spatio-temporal slope in the receptive field center (v_c , Eqn 5) in panel **b**. Pearson's coefficient (r) of correlation and Kendall rank correlation coefficient (τ) are r=0.62 ($p<0.02$), τ =0.47 ($p<0.02$) for **a** and r=0.77 (p=0.001) and τ =0.52 (p=0.01) for **b**.

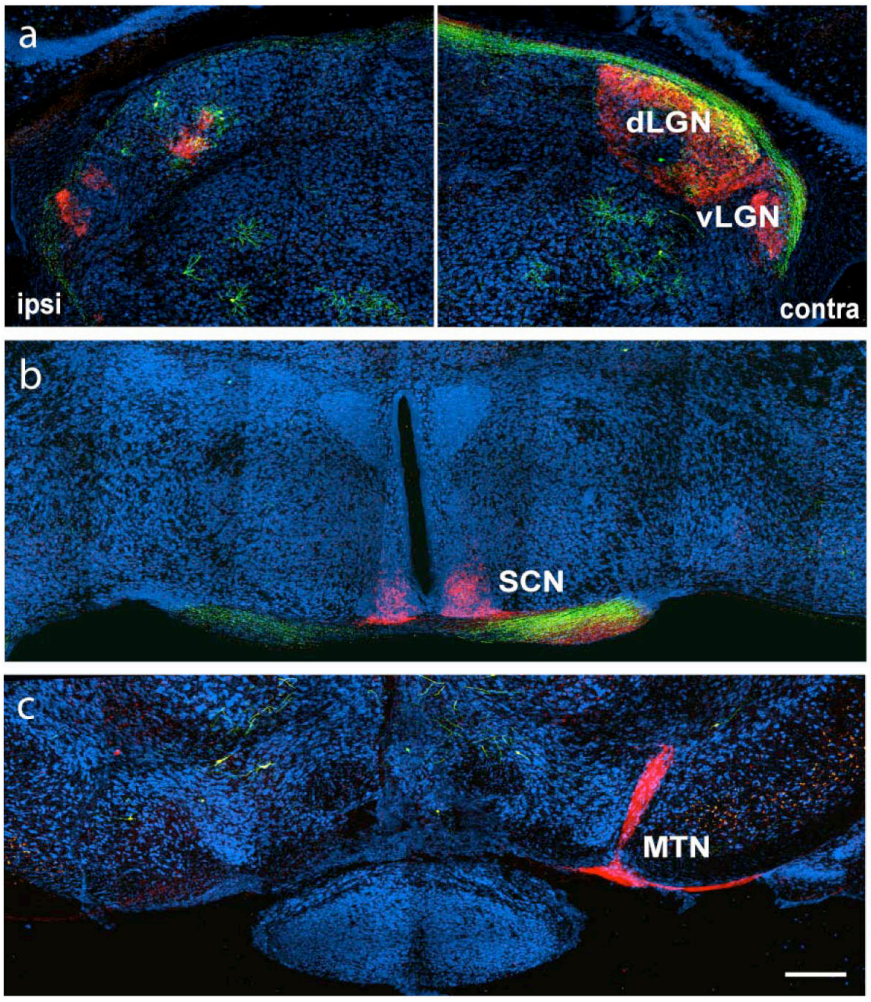

Supplementary Figure 7. Axonal arborizations of J-RGCs in the brain. Vibratome sections from JAM-B-CreER;Thy1-STOP-YFP mice were immunostained with anti-GFP. Axons of J-RGCs (green) terminate in dorsal lateral geniculate nucleus (dLGN; **a**) but not in ventral LGN (vLGN; **a**), suprachiasmatic nucleus (SCN; **b**), or medial temporal nucleus (MTN; **c**). All RGC axons were labeled by cholera toxin (red). One eye was removed 1 month before sacrifice. Scale bar is 250 μm.